NOTES AND CORRESPONDENCE

On the Differences between the Lifecycles of Some Baroclinic Waves Using the Primitive and Quasi-Geostrophic Equations on a Sphere

M. K. MACVEAN* AND I. N. JAMES

Department of Meteorology, Reading University, Reading RG6 2AU, U.K.

14 May 1985 and 1 November 1985

ABSTRACT

Lifecycles of baroclinic waves obtained by integrating the primitive and quasi-geostrophic equations on the sphere are compared. Two basic states are considered. The first is based on Northern Hemisphere winter climatology, while the other has a maximum baroclinicity at midlevels, but no temperature gradients on the upper and lower boundaries. The earlier part of the lifecycles are broadly similar for both equation sets, although there are significant quantitative differences. In the later stages, the momentum fluxes of the decaying waves can differ greatly. Moreover, we are unable to identify any systematic pattern in these differences. We conclude that the use of quasi-geostrophic results to parameterize the modification of the mean flow by baroclinic wave activity is likely to be subject to large errors.

1. Introduction

The transport processes associated with the growth and decay of baroclinic waves are of fundamental importance in the general circulation of the atmosphere (Lau, 1979). Most of the theories on which conceptual models of baroclinic instability are based use the quasi-geostrophic equation set. These equations are also used to derive important diagnostics of the large scale flow, such as the northward gradient of the zonally averaged quasi-geostrophic potential vorticity $[q]_y$ (which yields information about the stability of the flow to nonzonal perturbations) and the Eliassen-Palm flux (which indicates the propagation and mean flow interaction properties of the waves, see Edmon et al., 1980). The major assumptions made in deriving the quasi-geostrophic system of equations from the primitive equations are the neglect of horizontal variations of the static stability and the neglect of advection by the divergent flow. These assumptions are at best only approximately valid, even on the synoptic and longer timescales, and in many circumstances can be highly questionable. For example, the large low-level temperature fluxes in an unstable baroclinic wave lead to large variations of static stability, both in space and time. A further theoretical shortcoming of the quasi-geostrophic system is its handling of frontogenesis, which is an integral part of the lifecycles of baroclinically unstable waves (although it is poorly resolved by most numerical models, including those described in this paper). In the quasi-geostrophic system, the fronts have no tilt and there is no tendency for collapse to singularity in a finite time (Williams, 1972; Hoskins, 1982). In light of these considerations it is important to ask in what respects the quasi-geostrophic equations can reproduce the nonlinear lifecycles of baroclinic instabilities obtained using the primitive equation set. The question is also relevant to those who attempt to parameterize the effects of baroclinic waves on the larger scale flow.

Simmons and Hoskins (1976) compared the most unstable linear normal modes given by the quasi-geostrophic and primitive equations. Their calculations were based on a spectral model in spherical geometry. This study uses the same model, but extends the comparison to the nonlinear lifecycle of the baroclinic waves. Such lifecycles have been investigated in detail using the primitive equations by, for example, Simmons and Hoskins (1978). The present study is parallel to the work of Mudrick (1982) who used a finite difference model to represent a channel on the β-plane.

Our primitive equation model (PE) is the σ-coordinate hemispheric spectral model described by Hoskins and Simmons (1975). The quasi-geostrophic version (QG) was derived from it by suppressing advection by the divergent wind and by setting the static stability to a known function of the vertical coordinate only (Simmons and Hoskins, 1976). Both versions are adiabatic, apart from a ∇^6 linear horizontal diffusion operator applied to vorticity, divergence (in PE) and temperature. There is no orography but the full latitudinal variation of the Coriolis parameter is retained in both models.

The first set of results we describe uses an initial zonal flow based on climatological December–February flow for the Northern Hemisphere (hereafter designated DJF), as described by Oort and Rasmussen

* Present address: UK Meteorological Office, Bracknell RG12 2SZ, U.K.

(1971). The actual horizontal variation of static stability in this case is not especially large, and so we also present a complementary example in which the horizontal temperature gradients have a maximum in the mid-troposphere but are zero near the surface. In this internally unstable case (referred to as INT; it has been documented more fully by James and Hoskins, 1985) the surface static stability varies from near zero at high latitudes to nearly twice the global average at low latitudes. This case is a more stringent test of the effect of neglecting horizontal variations of the static stability in QG, whereas DJF emphasizes the effects of frontogenesis.

All our results were obtained using triangular truncation at total wavenumber 42. The DJF results are for zonal wavenumber 7 and five equally spaced levels in the vertical. The INT case had zonal wavenumber 9 and employed 15 equispaced levels in the vertical.

2. The DJF lifecycles

The perturbation to the initial zonal flow in the integrations described in this section was the most unstable linear normal mode, normalized to give a surface pressure amplitude of 1 mb. The development of the eddy kinetic energy (KE) and zonal kinetic energy (KZ) for both the PE and QG integrations is shown in Fig. 1. Qualitatively, both exhibit similar lifecycles. The initial period of roughly exponential baroclinic growth, with slight barotropic damping was followed by a period of equally rapid barotropic decay, when much of the wave energy was returned to the zonal flow. However, the energy does not decay monotonically to the end of the integrations; in each case a second, smaller amplitude cycle was observed. Since our aim was to examine the nonlinear development of the originally excited baroclinic wave, day 18 somewhat arbitrarily has been selected to represent the end of the lifecycle. In fact, there was some secondary development in the PE case before day 18; this is not apparent in the kinetic energy curve of Fig. 1, but was seen in the synoptic fields.

Up to day 8, during the exponentially growing phase of the cycle, PE and QG behave similarly. The QG growth rate is, however, about 10% smaller. Comparable and consistent differences were found in a DJF integration for zonal wavenumber 9, and for all wavenumbers in the Simmons and Hoskins (1976) study. The size of the difference is of the order expected from a Rossby number scaling, but the sign cannot be straightforwardly deduced from differences between the actual static stability in the region where growth occurs and the globally averaged values used in the QG integration.

The horizontal and vertical eddy fluxes of temperature and momentum are qualitatively and, in the case of the temperature fluxes, quantitatively similar. The time average eddy momentum fluxes are almost 50% smaller in QG. It should be remembered that since vertical advection is neglected in QG, the vertical fluxes in that case are implied rather than actual.

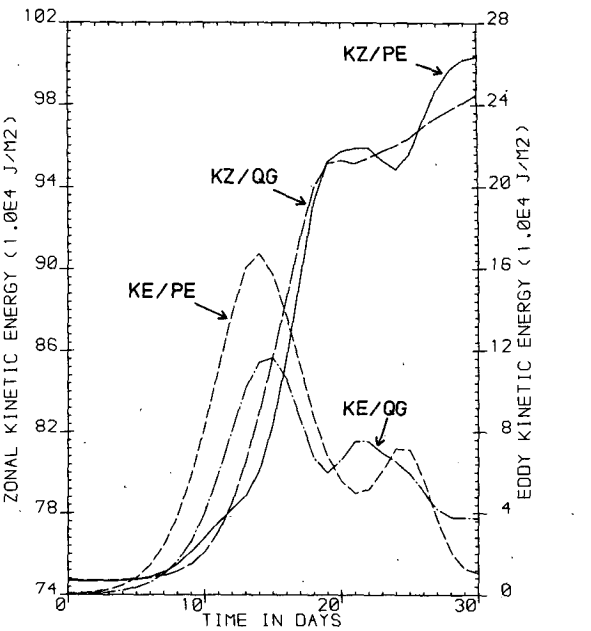

FIG. 1. The time development of the zonal (KZ), and wavenumber 7 (KE) kinetic energies in the PE and QG models, starting from the DJF initial state.

The maximum KE reached by PE is about 45% larger than for QG. This is partly related to the different linear growth rates, and partly to the secondary development which QG failed to capture. As the original wave grew to significant amplitude, its associated heat fluxes led to the formation of regions of enhanced baroclinicity on both flanks of the wave; it was on the poleward flank, between 50–60°N that the secondary PE disturbance grew. It reached a maximum amplitude at about day 14.

The changes that occurred in $[N^2]$ (the square of the Brunt-Väisälä frequency) over the lifecycle are shown in Fig. 2. The horizontal variation of $[N^2]$ in the lower troposphere at day 10 was much larger than in the initial state. The region around 30°N had been strongly stabilized, while that between 40° and 50°N had been destabilized. The fact that QG, with no vertical advection, produced similar changes in the actual static stability indicates that these changes must be due in large part to vertical variations in the horizontal temperature flux convergence, rather than variations of the vertical flux convergence.

Of course, the QG model does not respond to the predicted change of stability, so it is not surprising at first sight that it failed to reproduce the secondary development. This occurred in PE in the region of strong vertical and horizontal variations of static stability to the north of the location of the original wave.

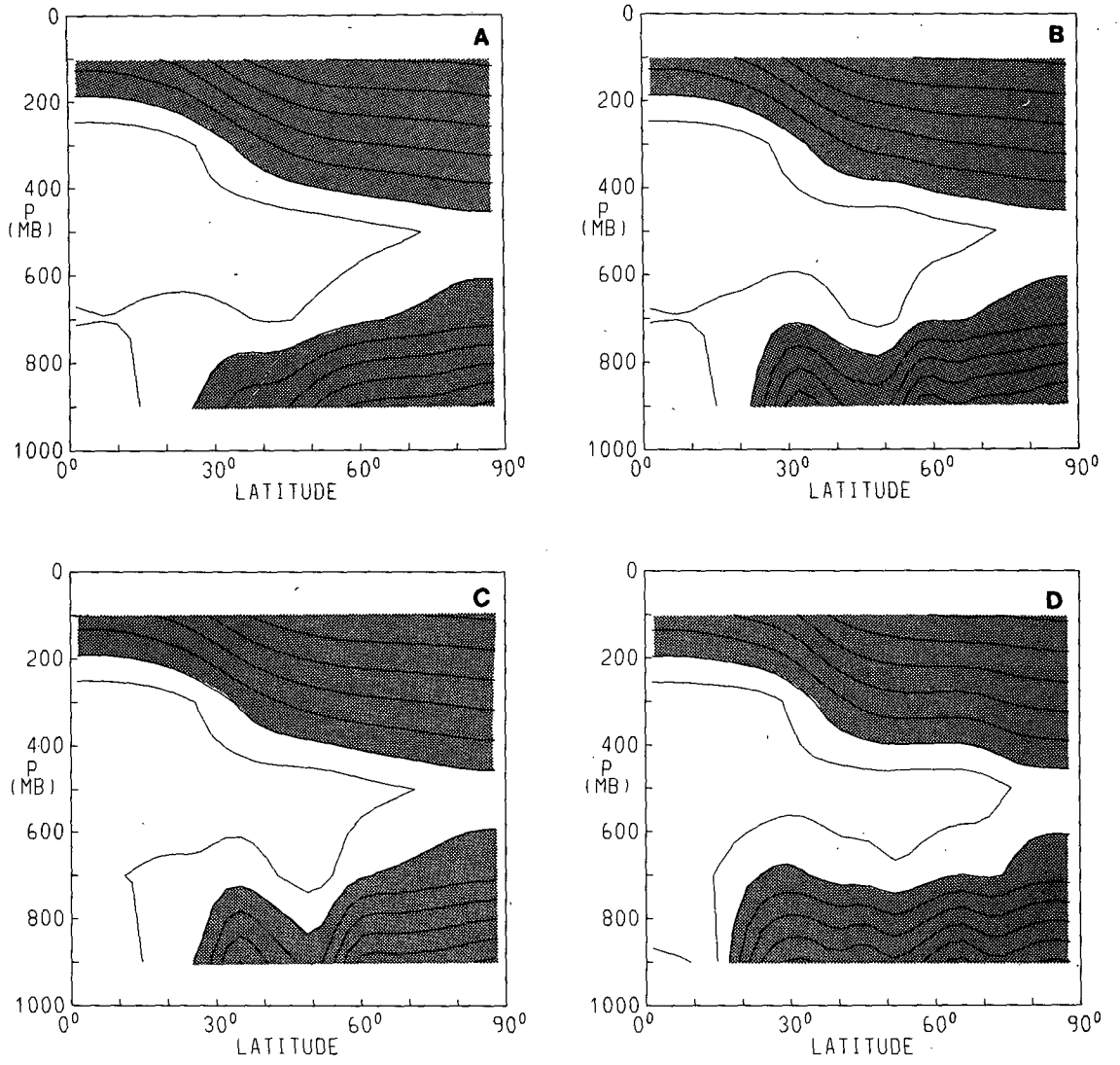

FIG. 2. $[N^2]$ for the DJF wavenumber 7 integrations: (a) initial state, (b) PE at day 10, (c) QG at day 10, (d) PE at day 18. Contour interval is 5×10^{-5} s^{-2}, and shading indicates values in excess of 2×10^{-4} s^{-2}.

Figure 3 shows $[q]_y$ for day 12, where

$$[q]_y = (1-\mu^2)\left\{\frac{2\Omega}{a} - \frac{1}{a^2}\frac{\partial^2([u]\cos\phi)}{\partial\mu^2}\right\} - 4\Omega^2\mu^2\frac{\partial}{\partial\sigma}\left\{\frac{\sigma^2 g^2}{R^2T^2g^2}\frac{\partial([u]\cos\phi)}{\partial\sigma}\right\} \quad (1)$$

and $\mu = \sin\phi$, ϕ being the latitude. The meridional coordinate, $y = a\ln(\sec\phi + \tan\phi)$, represents distance north on a Mercator projection of the globe. Other symbols have their conventional meaning. In QG, $[q]_y$ was calculated from the non-divergent zonal wind and horizontal mean static stability; it is a quantity of fundamental dynamical significance, appearing in the necessary condition for baroclinic instability. The calculation was generalized in PE to use the total zonal wind and the local static stability (a function of both σ and μ generally). Although it does not strictly have the same theoretical significance as the QG form, such a diagnostic has been found helpful in interpreting primitive equation results. The most significant differences between QG and PE are indeed seen in the region between 50° and 60°N, where the secondary development occurs. The differences in the $[q]_y$ fields can be related chiefly to the different static stabilities used in the two calculations. The differing $[q]_y$ fields do not, however, provide a clear explanation of why the secondary development is only apparent in PE. In conjunction with the fact that strong negative poleward surface temperature gradients exist locally, the $[q]_y$ fields imply that this region is a potential site for instability in both cases, although the unstable mode

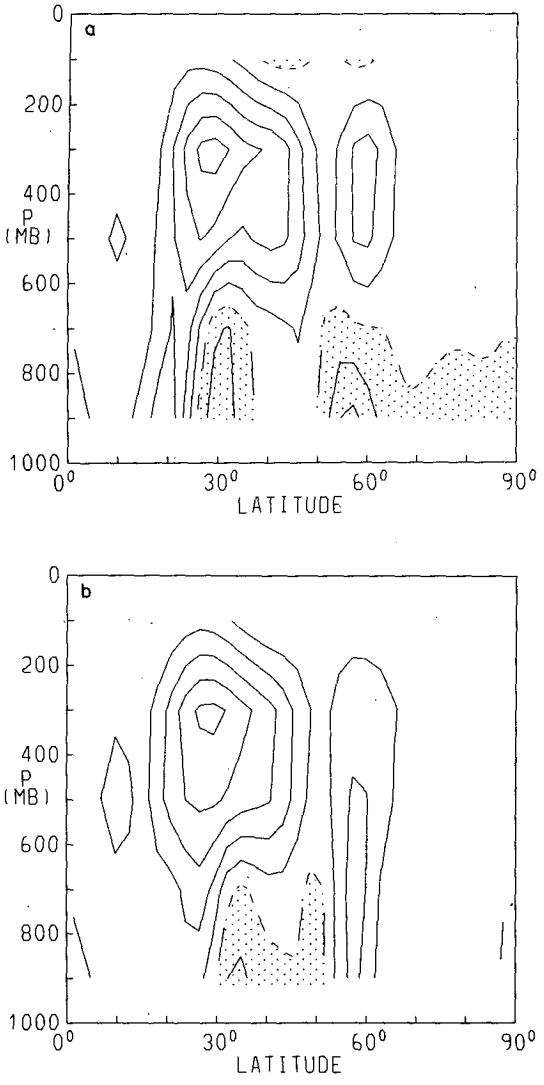

FIG. 3. $[q]_y$ at day 12 of the DJF wavenumber 7 integrations: (a) PE model, (b) QG model. Shading indicates negative values and the zero contour is dashed. Contour interval is 1.14×10^{-11} m^{-1} s^{-1}.

would have to be considerably deeper in PE to use the region of positive $[q]_y$.

Further evidence of how difficult it is to decide on the basis of such diagnostics whether or not an instability will occur is provided by a DJF lifecycle for zonal wavenumber 9. Similar differences in $[q]_y$ occurred but neither the QG or PE integrations exhibited secondary development.

In the barotropic decay phase of the waves, there are rapid conversions from eddy to zonal kinetic energy and an increase in the poleward momentum flux relative to the poleward heat flux in the upper troposphere. Since these fluxes are the equatorward and upward components of the Eliassen-Palm flux vector, the barotropic decay is manifested as a tilting of these vectors towards the equator, with convergence in the upper troposphere (Edmon et al., 1980). In contrast to these zonal wavenumber 7 results, there is no well-defined barotropic decay in the above sense in the DJF wavenumber 9 lifecycle; as the eddy energy decays so the zonal kinetic energy increases, but the Eliassen-Palm vectors turn downwards and slightly polewards. For both these wavenumbers, the decay phase in PE is qualitatively well reproduced in QG.

Finally we present some zonal mean quantities at the "end" of the lifecycle, that is, at day 18. The initial impression one gets from the zonal wind cross sections shown in Fig. 4 is the qualitative similarity between QG and PE. The maximum velocities attained are almost the same, both at 900 mb and 300 mb, but the

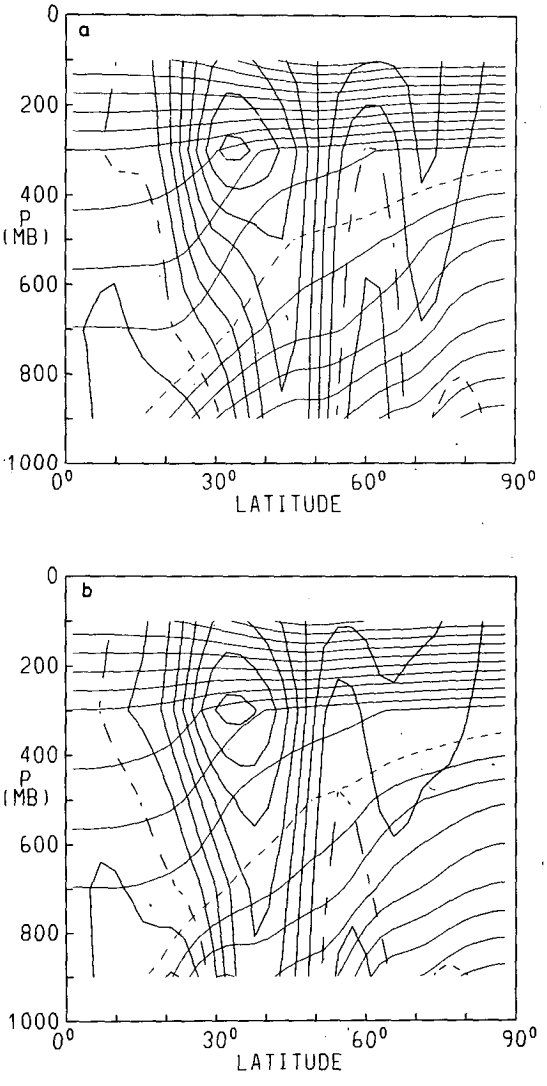

FIG. 4. Zonally averaged state at day 18 of the DJF wavenumber 7 integrations: (a) PE model, (b) QG model. The heavy lines are isotachs every 5 m s^{-1}, the main jet is westerly and the zero wind contour is dashed. The light lines are potential temperature with the 300 K contour dashed. Between this contour and the surface, the contour interval is 5 K; elsewhere it is 10 K.

low level maximum occurs at about 35°N in QG and 45°N in PE. Over much of the region between 30° and 70°N there are differences of 5–10 m s^{-1} between PE and QG, although this is mainly due to relatively small shifts in the position of regions of large horizontal gradients, reflecting chiefly the different horizontal eddy momentum flux distributions in the two cases.

The differences between the QG and PE temperature fields are mainly confined to low levels between 30° and 60°N. The PE atmosphere is significantly cooler there but it is a little warmer than the QG atmosphere on either side of this region. The magnitude of these differences is greater than that of the changes which occur during the PE lifecycle. As pointed out by Mudrick (1982), such a pattern of differences is to be expected in view of the constraint on the QG model to conserve the horizontal mean temperature at each level. One of the effects of secondary development in PE is to stabilize the region between 40 and 50°N, with the result that, in the extratropics, the final low level [N^2] (Fig. 2d) is much more uniform than in the initial state. In contrast, the static stability at the end of the QG run shows even greater horizontal variability than that illustrated in Fig. 2c, thus severely straining the assumption of uniform static stability in the model.

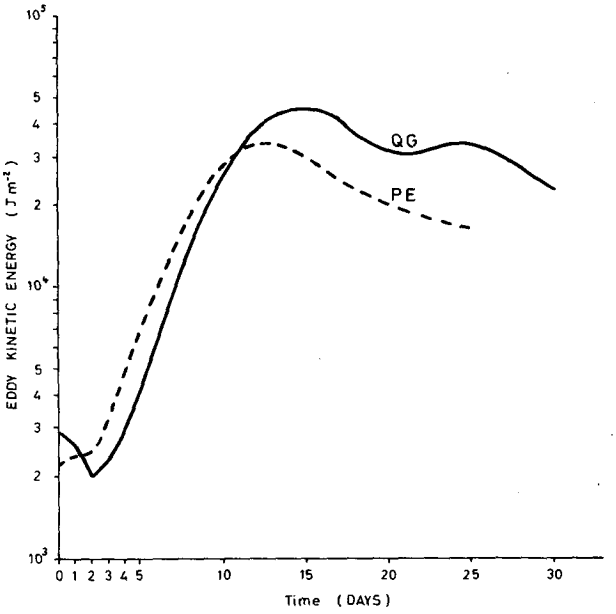

FIG. 5. The variation of eddy kinetic energy with time for the lifecycles beginning with the most unstable wavenumber 9 normal mode for the INT initial flow.

3. Internally unstable integrations

The INT initial state has a similar total baroclinicity to the DJF initial flow but a much greater variation of static stability over the meridional plane since the vertical scale of temperature variations is smaller. Low static stability is located at low levels poleward of the jet and at upper levels equatorward of it.

The models used for the INT integrations were identical to those used in the DJF runs, except that 15 equispaced levels were used to resolve the finer vertical structure properly. The initial zonal state was based on a zonal mean temperature field given by

$$T(\phi, \sigma) = T_s(\sigma) + \frac{\Delta T}{2} \sin(\pi\sigma) \tanh\left(\frac{30° - \phi}{10°}\right); \quad (2)$$

$T_s(\sigma)$ represents a reference temperature profile, chosen so that the corresponding value of N was 1.14×10^{-2} s^{-1}. The temperature difference between equator and pole ΔT was set to 16 K. The initial surface pressure was 1000 mb everywhere, and the zonal wind was obtained from the temperature and surface pressure distribution by solving the linear balance equation.

The initial zonal wavenumber 9 perturbation was formed from the corresponding 5-level normal mode structure by interpolation onto 15 levels. After about 3–5 days integration from a small amplitude, the structure of the perturbation became constant with its amplitude increasing exponentially, as illustrated in Fig. 5. Nonlinear effects were marked by day 9 of the integrations. A more detailed discussion of the form and nonlinear evolution of internal baroclinic waves is given by James and Hoskins (1984). In this note, we comment only on the differences between PE and QG.

The growth rate of the disturbance in PE was about 0.18 day^{-1}, while in QG it was slightly faster. Because it had to undergo more initial adjustment, QG spent less time in an exponentially growing state, and so its growth rate is less certain. Because of the strong dependence of growth rate on static stability (in Eady's theory, it varies as N^2) we anticipate a significant variation of growth rate between PE and QG. Because the scale of the horizontal variation of N is rather small compared to the width of the growing mode, it is not clear which value of N should determine the growth rate. Consequently, the changes of growth rate between the two cases are unpredictable.

In this case, QG achieved about 50% greater amplitude than PE. Mudrick (1982) also noted that QG achieved a larger amplitude at a later time than did PE. The subsequent decay process was markedly different, with a secondary development between days 21 and 26 in QG, but monotonic decay in PE. The pattern of Eliassen-Palm fluxes for the two cases is shown in Fig. 6. Both are taken for the time of maximum eddy available potential energy, which is also the time of maximum conversion from eddy available potential energy to eddy kinetic energy. At this stage, both integrations had comparable eddy kinetic energy. In neither case does the wave penetrate to the upper troposphere or propagate far in the meridional plane. This is similar to the DJF wavenumber 9 integrations, but in contrast to the DJF wavenumber 7 integrations described in section 2. In both PE and QG, the tilt of the

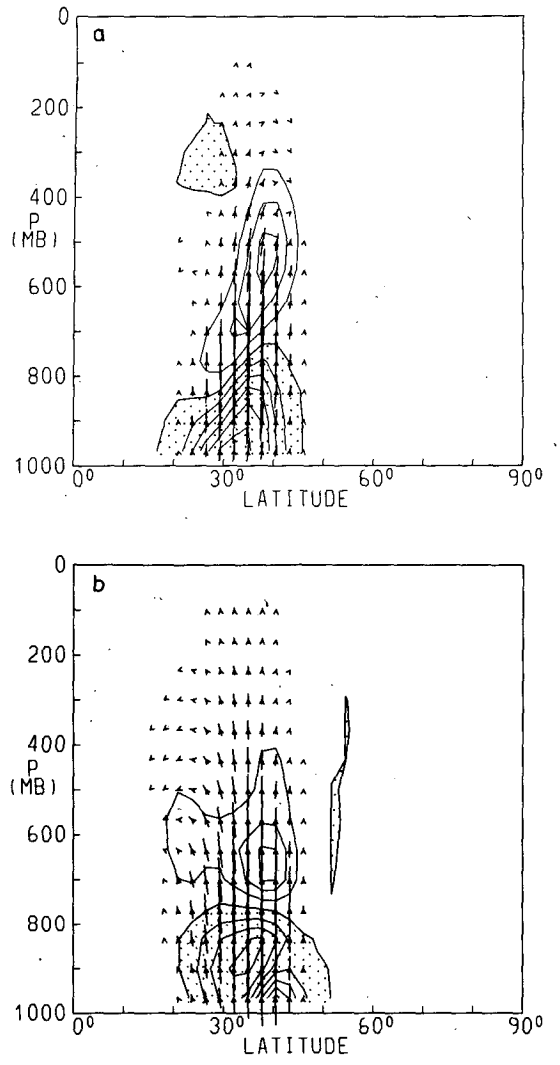

FIG. 6. Eliassen-Palm cross sections for the INT integrations. Both correspond to the time of maximum eddy available potential energy. (a) PE model at day 9. (b) QG model at day 12. Contour interval is 1.2×10^{15} m^3; shading indicates divergence of the Eliassen-Palm fluxes.

Eliassen-Palm vectors is small compared to that seen in the DJF runs. But while PE shows a small poleward component (i.e. equatorward momentum fluxes), QG shows larger and mostly equatorward tilts (poleward momentum fluxes).

The $[q]_y$ field at the end of the integrations, when the eddy fluxes had become insignificant, is shown in Fig. 7. The calculation was made in the same way as in section 2. The region of negative $[q]_y$ at low levels is split into two regions, to north and south of the latitude at which the wave growth was centered, in both QG and PE. The most prominent difference between the runs is the weakness of the northern $[q]_y$ minimum in QG. Although this partly reflects the different values of static stability used to compute the diagnostic in the two cases, it also is related to systematic differences in the $[u]$ and $[\theta]$ fields at the end of the integrations. It is interesting to note that the QG run showed the strong secondary development in the region of the northern $[q]_y$ minimum, despite the relative weakness of the potential vorticity variations. On the basis of the $[q]_y$ fields, the PE rather than the QG run might have been expected to undergo a secondary development.

Figure 8 summarizes the differences in the $[u]$ fields at the end of the lifecycles. The jet is stronger and further north at the end of PE. This is a direct result of the convergence of the momentum fluxes near 35°N in this integration. In contrast, QG shows stronger surface easterlies to the north of the jet. In the same way, the deceleration of the westerlies to the south of the jet is more marked in PE. These contrasts both arise from

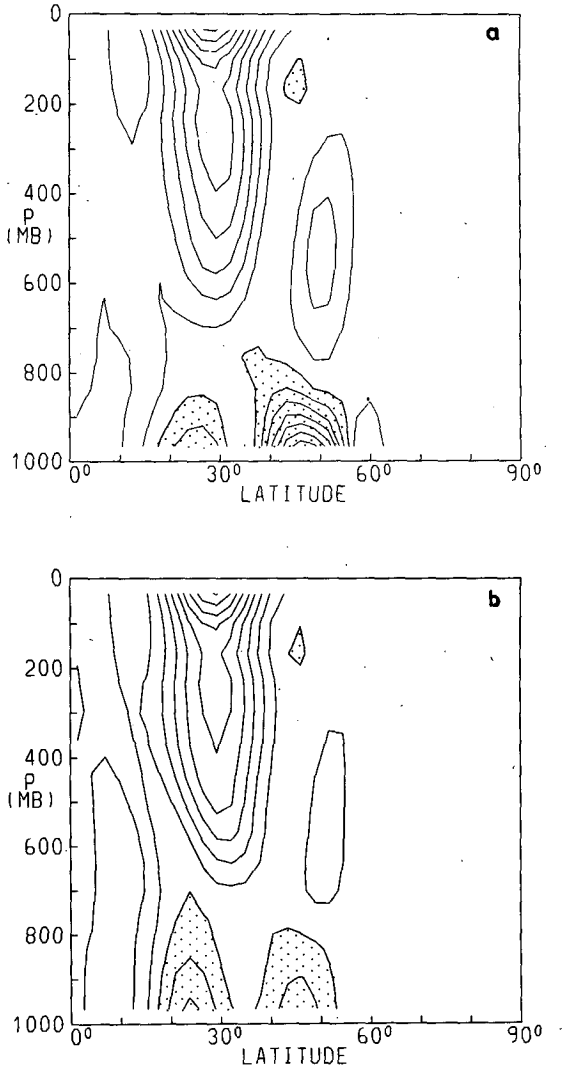

FIG. 7. $[q]_y$ at the end of (a) the PE integration and (b) the QG integration with the INT initial data. Contour interval is 1.14×10^{-11} m^{-1} s^{-1}; shading indicates negative $[q]_y$.

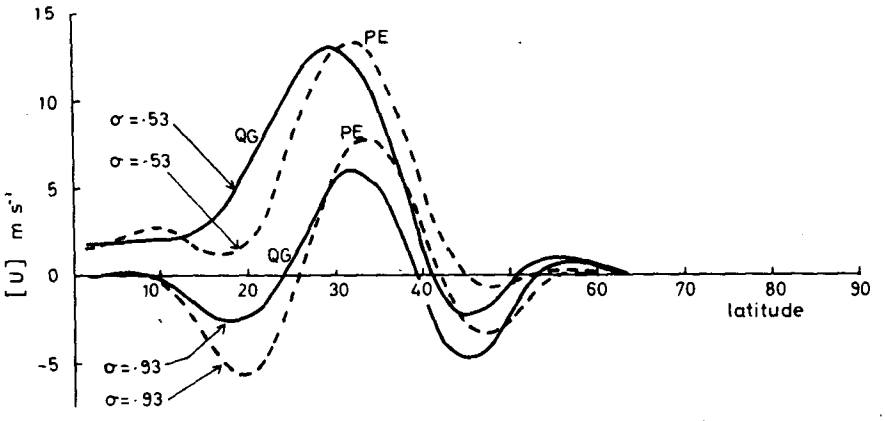

FIG. 8. $[u]$ near the surface ($\sigma = 0.93$) and near the middle troposphere ($\sigma = 0.53$) at the end of the integrations from the INT initial state.

the oppositely directed eddy momentum fluxes in the two cases.

4. Conclusions

In broad terms, the lifecycles exhibited by the PE and QG models are similar, despite the neglect of vertical advection and of horizontal and time variations of static stability in QG and its known deficiency in handling frontogenesis. In fact, frontogenesis appears to be a rather unimportant feature of the large scale flow during the nonlinear phase of the lifecycle. But it must be noted that the horizontal resolution used in these models is scarcely enough to resolve frontal structures. In both PE and QG runs with the DJF initial state, the extreme relative vorticities in the frontal region were only of the order of $\pm 0.5f$. According to Williams (1972) and Hoskins (1982), the deficiencies of the QG model in regard to frontogenesis are not likely to be crucial at such levels of relative vorticity. There is evidence that the maximum vorticity was limited to this level by the resolution and dissipation used. Earlier in the integration, there was a clear bias in the PE model towards positive relative vorticity which was not present in the QG case. This bias, which is predicted by semi-geostrophic theory (Hoskins, 1982), disappeared as the relative vorticity approached 0.5f. The INT lifecycles are not expected to lead to frontlike structures, since they have no low-level temperature gradients to amplify.

At a more detailed level, there are significant differences between PE and QG. The linear growth rates are appreciably different for a given initial state, as are the maximum amplitudes reached by the wave, the magnitude and even the direction of the momentum fluxes and the degree of secondary instability generated on the poleward flank of the jet. We are unable to see any systematic pattern in these differences. Indeed, the DJF and INT integrations reported here show contrary changes in all the respects noted above when the PE equations are replaced by the QG equations. It is difficult to use simple arguments to relate these differences to, for example, variations of static stability, and the most we would claim is that order Rossby number differences between integrations with the two equation sets are expected, but that the sign of the difference is not predictable. Table 1 outlines some of the major contrasts between our integrations, and also includes some of Mudrick's (1982) conclusions.

During the growing stage of the lifecycle, the modification of the basic flow is achieved principally by heat fluxes. As Mudrick pointed out, the heat fluxes are similar in both the PE and QG integrations. During the later decay stage, the momentum fluxes become

TABLE 1. A summary of our results, compared to those of Mudrick (1982 and 1985, personal communication).

Property	DJF	INT	Mudrick
Linear growth rate	PE > QG	PE < QG	Variable
Maximum amplitude of KE	PE > QG	PE < QG	PE < QG
Dominant direction of $[u^*v^*]$	N in PE and QG ($m = 7$) S in PE and QG ($m = 9$)	N in PE S in QG ($m = 9$)	Generally S in PE and QG ($m = 6, 8$)
Magnitude of $[u^*v^*]$	PE > QG	Similar in PE & QG	PE > QG
Secondary development	Only in PE	Only in QG	State 1: PE only State 2: PE and QG

larger and the heat fluxes decline; the modification of the basic state is then strongly dependent upon the momentum fluxes. The magnitude and even the sign of the momentum fluxes are highly variable, depending both on the equation set used and the details of the initial state. Gall (1977) pointed out that the heat fluxes are much less sensitive than the momentum fluxes to the detailed structure of the disturbance (and hence to the equation set employed) in the linear stage. Similarly, cancellations are involved in the calculation of the momentum flux in the nonlinear phase and it is not surprising that this sensitivity is important throughout the lifecycle.

Such sensitivity implies that the use of QG rather than PE dynamics to parameterize the total effects of baroclinic waves in low resolution, long term integrations would lead to significantly different model climatologies. In contrast, by concentrating on the heat fluxes, Mudrick concluded that the lifecycles are relatively insensitive to the equation set used. This led him to suggest, with certain caveats, that QG dynamics could be useful in baroclinic wave parameterizations.

In this study, we have restricted our attention to the interaction between a single zonal wavenumber (and its harmonics) and the zonal flow. In a more complex system, wave–wave interactions are important in the equilibration of the eddy energy (e.g., see Mak, 1985). Even in such a system, we would expect the strength and direction of the zonal mean momentum fluxes to exhibit the same sensitivity to the equation set employed.

Finally, we note that the vertical heat fluxes in PE lead, as expected, to an overall stabilization of the lower troposphere. But, at least during the limited period covered by a lifecycle integration, much of the dynamically significant variation of static stability can be attributed to vertical variations of the poleward temperature flux convergence. This mechanism is active in both the PE and QG models.

Acknowledgment. We thank Dr. Mudrick for his helpful and detailed comments on an earlier draft of this note.

REFERENCES

Edmon, H. J., B. J. Hoskins and M. E. McIntyre, 1980: Eliassen-Palm cross sections for the troposphere. *J. Atmos. Sci.*, **37**, 2600–2616.

Gall, R., 1977: Some non-quasi-geostrophic effects in linear baroclinic waves. *Mon. Wea. Rev.*, **105**, 1039–1051.

Hoskins, B. J., 1982: The mathematical theory of frontogenesis. *Ann. Rev. Fluid Mech.*, **14**, 131–151.

——, and A. J. Simmons, 1975: A multilayer spectral model and the semi-implicit method. *Quart. J. Roy. Meteor. Soc.*, **101**, 637–655.

James, I. N., and B. J. Hoskins, 1985: Some comparisons of atmospheric internal and boundary baroclinic instability. *J. Atmos. Sci.*, **42**, 2142–2155.

Lau, N.-C., 1979: The structure and energetics of transient disturbances in the Northern Hemisphere wintertime circulation. *J. Atmos. Sci.*, **36**, 982–995.

Mak, M., 1985: Equilibration in nonlinear baroclinic instability. *J. Atmos. Sci.*, **42**, 2764–2782.

Mudrick, S. E., 1982: A study of the adequacy of quasi-geostrophic dynamics for modeling the effect of cyclone waves on the larger scale flow. *J. Atmos. Sci.*, **39**, 2414–2430.

Oort, A. H., and E. M. Rasmussen, 1971: Atmospheric circulation statistics. NOAA Prof. Paper 5, U.S. Dept. of Commerce.

Simmons, A. J., and B. J. Hoskins, 1976: Baroclinic instability on the sphere: normal modes of the primitive and quasi-geostrophic equations. *J. Atmos. Sci.*, **33**, 1454–1477.

——, and ——, 1978: The lifecycles of some nonlinear baroclinic waves. *J. Atmos. Sci.*, **35**, 414–432.

Williams, R. T., 1972: Quasi-geostrophic versus nongeostrophic frontogenesis. *J. Atmos. Sci.*, **29**, 3–10.